Highlights

Synoptic patterns and mesoscale precursors of Italian tornadoes

Leonardo Bagaglini, Roberto Ingrosso, M. M. Miglietta

- Peculiar synoptic conditions associated with Italian tornadoes for different regional clusters are identified;
- Relevant anomalies of both synoptic and mesoscale precursors occur during tornado events; environmental conditions favorable to tornado development differ among the southern and northern Italian regions;
- Tornadoes in southern regions are characterised by the highest anomalies in wind shear and CAPE;
- Sea surface temperature anomalies seem to play a significant role for southern and northern Adriatic tornadoes.

Synoptic patterns and mesoscale precursors of Italian tornadoes

Leonardo Bagaglini[a], Roberto Ingrosso[b,*], M. M. Miglietta[c]

[a]*ISAC-CNR, Istituto di Scienze dell'Atmosfera e del Clima - Consiglio Nazionale delle Ricerche, Roma (Italy)*
[b]*Department of Earth and Atmospheric Sciences, University of Quebec in Montreal (UQAM), Montreal, QC, (Canada)*
[c]*ISAC-CNR, Istituto di Scienze dell'Atmosfera e del Clima - Consiglio Nazionale delle Ricerche, Lecce/Padua (Italy)*

Abstract

An analysis of synoptic patterns and mesoscale precursors is produced for Italian tornadoes for the period 2000–2018. Anomaly maps of different parameters are extracted from ERA-5 reanalysis. To highlight typical large-scale configurations, a clustering analysis is applied to define different regional clusters, representative of areas affected by a large number of tornadoes. The analysis shows that: a) significant anomalies of synoptic parameters and mesoscale precursors are generally present over and nearby the region where tornadoes occur; b) each cluster shows a peculiar synoptic configuration; c) pattern differences among clusters suggest different environmental conditions favorable to tornado development in the southern and northern Italian regions; d) tornadoes in southern regions are characterised by the highest anomaly values in wind shear, storm relative helicity and CAPE; e) significant SST positive anomalies are observed for southern tornadoes.

*Corresponding Author
Email addresses: Leonardo.Bagaglini@artov.isac.cnr.it (Leonardo Bagaglini), ingrosso.roberto@courrier.uqam.ca (Roberto Ingrosso), m.miglietta@isac.cnr.it (M. M. Miglietta)

Keywords: Tornado, Precursors, Synoptic scale, Statistical Analysis, ERA-5, Clustering, Sea surface temperature, Anomalies,

1. Introduction

Tornadoes are one of the more fascinating and fierce weather phenomena on Earth. Accordingly with the World Meteorological Organization, a tornado consists in a rotating column of air, extending from the base of a cumuliform cloud to the ground, characterized by winds exceeding $29\,m\,s^{-1}$. Although the number of intense tornadoes affecting the Italian regions is not negligible, the topic rarely has been the subject of scientific investigation. However, in the recent years, the concern for the danger related to these phenomena has increased after that strong tornadoes hit some areas of the peninsula, causing fatalities and significant damage (Miglietta and Rotunno, 2016; Zanini et al., 2017; Miglietta et al., 2017b). Italian tornadoes occur mainly over flat terrains, the Tyrrhenian and southern coasts; in contrast the central Adriatic coast and Sardinia count a very small number of events (Palmieri and Pulcini, 1978; Gianfreda et al., 2005; Giaiotti et al., 2007; Miglietta and Matsangouras, 2018; Ingrosso et al., 2020).

The rating of tornado intensity is based on damage survey. A first attempt of classification, the so called Fujita or F-scale, was introduced by Fujita (1971), but this scale was difficult to apply and somehow inaccurate. Different scales were proposed afterward, such as the fine Torro scale in 1976 (Meaden, 1976), mainly applied in the UK, and the Enhanced Fujita scale (EF; Potter (2007)), an update of the F-scale, which provides a better estimate of the damage, but relative to buildings in the USA and Canada. The EF-scale classifies tornadoes into six categories, based on their impact on vegetation, buildings and vehicles, ranging

from EF0 (weak damage) to EF5 (almost complete destruction).

The study of tornadoes in the scientific literature is generally based on observations (e.g. weather radar and soundings) and model reanalyses. The latter are useful to describe the atmospheric state favouring the formation of severe thunderstorms, but their usage is limited by their coarse resolution, which is not able to completely resolve the mesoscale features characterizing tornado events. However, due to the sparsity of direct observations, they usually provide the only valuable source of information to investigate the environment where tornadoes originate and develop. Brooks et al. (2003) and Brooks (2009) used the National Centers for Environmental Prediction (NCEP) reanalysis (Kalnay et al., 1996) from National Center for Atmospheric Research (NCAR) to analyse some parameters associated with severe thunderstorms in US. With regard to the European region, Romero et al. (2007) used ERA-40 (Uppala et al., 2005) from European Centre for Medium-Range Weather Forecasts (ECMWF) for the analysis of environmental parameters related to severe convective storms in Europe. Taszarek et al. (2018) used the ERA-Interim reanalysis from ECMWF, comparing these data with over 1 million sounding measurements in the European region, whereas Ingrosso et al. (2020) applied both ERA-Interim and ERA-5, the recently issued higher resolution reanalysis from ECMWF (Hersbach et al., 2020), to the Italian area. Renko et al. (2013) and Matsangouras et al. (2014) characterised the synoptic environment where tornadoes develop by means of ERA-INTERIM for the Eastern Adriatic basin and NCEP-NCAR reanalysis for Greece, respectively. ERA-5 was also recently used by Rodríguez and Bech (2020) in their analysis of tornadic environments over the Iberian peninsula.

In the present article, we investigate synoptic patterns associated with torna-

does in different Italian regions. The literature about southern Europe tornadoes focused on the synoptic-scale conditions associated with the tornado events is very limited (Sioutas and Keul, 2007; Keul et al., 2009; Renko et al., 2013; Matsangouras et al., 2014). Sioutas and Keul (2007) detected synoptic patterns favorable to waterspouts development in the Adriatic, Ionian and Aegean Sea. Four synoptic categories were found, based on the 500 hPa flow, defined accordingly with the position and orientation of trough and ridge axes and surface features: the south-west flow (SW), the long-wave trough (LW), the short-wave trough (SWT) and the closed low (CLOSED). Considering the whole region, they found that CLOSED, followed by LW, was the dominant type in waterspout occurrences. The conclusions of Keul et al. (2009) for the same regions slightly differed from Sioutas and Keul (2007), since the SW and CLOSED represent the dominant types in their study. Results consistent with Sioutas and Keul (2007) were shown by Renko et al. (2013) for the Eastern Adriatic basin. Matsangouras et al. (2014) analysed three different Greek sub-regions in autumn, when tornadoes and waterspouts are most frequent. They found a typical synoptic configuration for tornadoes over west Greece, i.e., a trough over southern and central Italy at 500 hPa accompanied by a closed cyclonic circulation over the Gulf of Taranto, while a trough over the eastern Aegean Sea is the synoptic pattern for waterspouts North of Crete.

Few papers also looked at the role of the sea surface temperature (SST). Matsangouras et al. (2014) suggested that positive SST anomalies were responsible for the significant number of waterspouts over the Aegean Sea in summer 2002, when the SST was $1^{\circ}C$ higher than the 1985-2008 climatology of the basin (Skliris et al., 2011). A relevant role of SST anomalies was also found in Miglietta et al. (2017b), who detected significant changes in updraft helicity and vertical velocity

associated with small variations of SST for a waterspout making landfall over the Ionian coast of Apulia region. Similar results were recently shown by Marín et al. (2020), who pointed at the small SST variations for the ~~increasing~~increased atmospheric instability responsible for the storm severity during tornadoes in central-southern Chile. Finally, Molina et al. (2020) showed, for a tornado outbreak in the Southeast USA, that, during the first day of the event, warmer SST increased tornado frequency while cooler SST reduced tornado activity.

Operative numerical weather prediction models (NWP models) are not able to completely resolve the characteristic spatio-temporal scales of a tornado event (of the order of tens/houndreds of metres on the horizontal, few hundreds metres on the vertical and living for several tens of minutes), thus they are not reliable for predicting tornado occurrences with a high accuracy degree. Therefore, environmental variables such as the vertical wind shear (WS), the convective available potential energy (CAPE), the storm relative helicity (SRH) and the low-level moisture, which have been identified as reliable tornado precursors and indicative of environmental conditions favourable to severe convective weather, are carefully monitored and analysed (Davies and Johns, 1993; Brooks et al., 2003; Thompson et al., 2003; Craven and Brooks, 2004; Brooks, 2013; Taszarek et al., 2017). In the same spirit, combined thermodynamics and kinetic parameters were also considered in several studies concerning tornadoes (Rasmussen and Blanchard, 1998; Brooks et al., 2003; Craven and Brooks, 2004; Allen et al., 2011; Púčik et al., 2015).

Colquhoun and Shepherd (1989) analysed the US tornadoes and found a statistically significant relationship between deep level qind shear (DLS) and tornado intensity, with a minor role of relative helicity and mid-tropospheric relative hu-

midity. Markowski and Richardson (2014) showed that tornadic supercells are also favoured also by high low-level relative humidity; the latter could play a significant role in increasing the buoyancy in the rear flank downdraft (Markowski et al., 2002; Thompson et al., 2003). Thompson et al. (2003) found that both CAPE and low-level wind shear (LLS), as well as SRH in the lowest 0-1 km layer, represent good discriminators between tornadic and non-tornadic supercells. Dupilka and Reuter (2006) and Brooks (2013) showed that in the USA the key factor for a tornado occurrence is the DLS, while CAPE seems to play a fundamental role for the formation of severe thunderstorms in general.

Regarding the European tornadoes, Grünwald and Brooks (2011) found that the combination of high values of WS and CAPE discriminates between weak and significant tornadoes. Taszarek et al. (2017) showed that vertical shear, 0–1 km SRH and CAPE are good predictors of tornadic thunderstorms; among the shear parameters, the mid-level shear (MLS) better distinguishes between weak and relevant tornadic events. The wind shear is the most promising predictor to discriminate between weak and significant tornadoes in central Europe (Púčik et al., 2015); SRH is also a good discriminator between the two categories. On the other hand, CAPE discriminates only between no tornadoes and weak tornado occurrences. Rodriguez and Bech (2017) analysed tornadoes in different regions of Iberian peninsula. They found that, for Catalunia, 0-3 km SRH and WS are good discriminators among non-tornadic, weak tornadic and significant tornadic thunderstorms. The SB (Surface Based) CAPE was a good indicator related to convection development, but its values do not differ significantly among different kinds of tornadic thunderstorms. Similar results were obtained in Groenemeijer and van Delden (2007) for Nederlands and Taszarek and Kolendowicz (2013) for

Poland. In general, the European region shows lower values of CAPE compared to North America, as shown by Rasmussen and Blanchard (1998); Grams et al. (2012) and recently by Taszarek et al. (2020), who carried out a systematical analysis of the environmental conditions characterizing the severe convective storms in both US and Europe Ingrosso et al. (2020) showed that the probability of tornado occurrence in Italy significantly increases with the magnitude of LLS and DLS in an environment characterised by medium-to-high values of WMAX. In particular, in Italy, low-. WS seems to play a predominant role in the formation of tornadoes (Giaiotti et al., 2007; Miglietta and Rotunno, 2016; Miglietta et al., 2017a; Ingrosso et al., 2020). Ingrosso et al. (2020) also found that the vertical WS and CAPE generally take on values larger than the mean climate conditions just before the occurrence of a tornado. Here, the analysis is extended to include other potential precursors.

In particular, in this article we investigate the existence of specific synoptic patterns, in different Italian regions hit by tornadoes, and analyse the typical environmental conditions prior to tornado occurrence. Firstly, high frequency tornado *hot-spots* are detected. This enabled the identification of geographical clusters, in which tornadic events occur more frequently. These preliminary clusters, however, share a certain degree of similarity in the underlying synoptic conditions, allowing to merge those sufficiently akin. Once the definitive clusters are identified, a mean atmospheric state for each cluster is defined and anomaly and standardised indices fields are drawn and analysed to check the potential deviation from the mean climatological state of each tornadic cluster. In order to rationalise the choice of the relevant variables to consider, we train an ensemble learning model (specifically a random forest) aiming to identify the variables showing the

most anomalous patterns (with respect to standard, non-tornadic, conditions). In addition, distributions of real values and standardised indices are investigated by means of violin plots to compare different precursors and highlight their singularity in the 1-hour closest to the event. The analysis of the chosen average variables, on one hand, allows the characterisation of synoptic states favourable to tornado generation and, on the other, gives a more complex picture of the inner dependencies among parameters and processes. However, while certain variables show unequivocal signals associated to tornado occurrence and intensity, others manifest ambiguous characters, depending on the geographic location.

The paper is structured as follows. In Section §2 we describe the dataset and the area of interest (§2.1) and we explain the clustering method applied to group tornado events into clusters (§2.3). Then, in Section §3, we present the main results of the article. Precisely, we describe the synoptic states and analyse the mesoscale precursors characterizing the tornadic activity of each cluster in §3.1 and §3.2 respectively. The next section is devoted to analyse the results, to highlight some relevant implications and to suggest new research lines for future studies (§4).

2. Data and Methods

2.1. Datasets and area of study

The list of Italian tornadoes, used in this study, derives from the dataset validated in Miglietta and Matsangouras (2018) for the analysis of tornadoes in Italy for the period 2007–2016 and extended to the period 2000–2018 in Ingrosso et al. (2020). The dataset represents an integration of the European Severe Weather Database (ESWD, https://www.essl.org), managed by the European Severe Storm

Laboratory (ESSL), with other reports by weather amateurs, national and local newspapers including videos and pictures. This analysis is restricted to EF1+ (category EF1 or higher) tornadoes, since EF0 are characterized by weaker synoptic forcing (e.g., weak watespouts reaching the coasts), which may add noise to the dominant features. Regarding the meteorological parameters, the reanalysis dataset used here is ERA-5, the recent high–resolution reanalysis from ECMWF (Hersbach et al., 2020), with a temporal resolution of 1 hour, spatial resolution of $0.25° \times 0.25°$ and 137 vertical levels from the surface up to 0.1 hPa. The area considered in the study is relative to the Italian region (32°N-50°N and 3°E-22°E).

2.2. Definitions

2.2.1. Meteorological parameters

The meteorological parameters used in this study are either directly extracted from the ERA-5 reanalysis or calculated from its variables. They include:

i. Horizontal Wind $\mathbf{u}$;
ii. Geopotential Height z ;
iii. Mean Sea Level Pressure $mslp$;
iv. Temperature t and Dew-point Temperature t_d ;
v. Specific Humidity q ;
vi. Vertical Wind Component w ;
vii. Convective Available Potential Energy CAPE.

2.2.2. Vertical Wind Shear

Given a prescribed pressure level p, the Vertical Wind Shear WS at p is defined as

$$\mathrm{WS}_p = \|\mathbf{u}_p - \mathbf{u}_{10m}\|,$$

where $\mathbf{u}_p$ and $\mathbf{u}_{10m}$ are the horizontal wind fields at pressure level p and $10\,m$ above the surface respectively, and $\|\cdot\|$ denotes the Euclidean norm.

In the present study we often refer to three distinct characterizations of WS, namely: the low-level shear $\mathrm{WS}_{900\,hPa}$ (LLS), the mid-level shear $\mathrm{WS}_{700\,hPa}$ (MLS) and the deep-level shear $\mathrm{WS}_{500\,hPa}$ (DLS)[1].

2.2.3. Storm Relative Helicity

Storm Relative Helicity is the vertical integral, taken from the ground level z_{sf} to a given height $z(p)$, of the scalar product between the horizontal flow motion relative to the storm and the vorticity of the horizontal wind, that is:

$$\mathrm{SRH}_p = \int_{z_{\mathrm{sf}}}^{z(p)} (\mathbf{u} - \mathbf{SM}) \cdot (\nabla \times \mathbf{u})\, d\zeta,$$

where **SM** is the storm motion relative to the ground (parameterised accordingly with Kaltenböck et al. (2009)), and $\nabla \times \cdot$ denotes the curl operator of the Levi-Civita connection of the three-dimensional euclidean space.

SRH is the integral measure of the streamwise vorticity of the flow relatively to the storm. When vorticity and storm relative wind are aligned, the local tilting of isentropic surfaces, as in the presence of severe convection, leads to cyclonic vertical updraft currents (Davies-Jones, 1984). This process causes the development of supercell storms and the formation of meso-cyclones, whence the significance of SRH.

In this study, we considered SRH in two different layers, namely $\mathrm{SRH}_{700\,hPa}$ and $\mathrm{SRH}_{900\,hPa}$.

[1] In the calculation of wind shear, we keep the pressure levels as extracted from ERA-5 to avoid interpolations at heights usually considered in the definition of LLS, MLS and DLS.

2.2.4. Lifting Condensation Level

The Lifting Condensation Level LCL is a common measure of the level of condensation derived within the Parcel Theory. Its exact computation, however, is not straightforward as it depends on several assumptions on the atmosphere stratification (see Romps (2017) for a recent survey). The formal definition is the altitude at which an air parcel, generally taken at ground level, has to be (isentropically) lifted for saturation to occur. Since we were interested in studying the LCL variations on large scales we chose to adopt the Espy's approximation, as optimised in Lawrence (2005):

$$\mathrm{LCL} = (125\,m/K) \cdot (t_{10m} - t_{d10m})\,,$$

where t_{10m} and t_{d10m} are the temperature and dew-point temperature (in K) at $10\,m$ above the surface, respectively. This rough approximation is easy to implement and, despite its simplicity, it is able to capture the leading order variations of LCL. Therefore, it represents a good compromise to highlight relevant patterns on large scales.

2.2.5. CAPE and Updraft Maximum Vertical Velocity

CAPE (Moncrieff and Miller, 1976; Doswell and Rasmussen, 1994; Emanuel, 1994) represents a measure of the available potential energy. It is defined as

$$\mathrm{CAPE} = \int_{LFC}^{EL} B\,dz,$$

where z is the height, $B = g\frac{T_{Vp}-T_{Ve}}{T_{Ve}}$ is the buoyancy force, LFC is the Level of Free Convection, EL is the Equilibrium Level, and T_{Vp} is the virtual temperature of an air parcel and T_{Ve} the virtual temperature of the environment. In ERA-5, CAPE represents the maximum value among the air parcels lifted from different

model levels below 350 hPa (MUCAPE). CAPE is considered a standard meteorological variable, used for both forecast and analysis purposes, therefore it is an obvious choice for studying synoptic and mesoscale configurations. Generally, CAPE takes values ranging from tens to thousands of $J \cdot kg^{-1}$. The maxima, however, turn out to be very rare, occurring only in condition of extreme instability. Consequently standardised indices of CAPE tend to be very sensitive to outliers (large CAPE). For this reason we also used the equivalent form of CAPE given by WMAX, as for the analysis of the local distributions within §2.4. WMAX is used here supposing that buoyancy is the only active force accordingly to the Parcel Theory ((Holton, 2004; Markowski and Richardson, 2010)) and is equal to:

$$\text{WMAX} = \sqrt{2 \cdot \text{CAPE}}.$$

2.3. Clustering

Among the 570 tornadoes within the reference dataset (only tornadoes over land are included, including waterspouts making landfall), occurred between the years 2000 and 2018, we selected only 149 of them, with a time uncertainty no greater than 2 hours and intensity greater than or equal to EF1, 114 of category EF1[2] and 35 of category EF2 or higher (EF2+). The time threshold was chosen to prevent the noise emerging from a inaccurate (early or late) representation of the environmental conditions.

As we were interested in finding synoptic conditions favouring tornadic activity, we initially defined 10 local clusters of nearby events (Figure 1, left panel) using an optimum density criterion. Then, to reduce their number and, in turn,

[2]Only 149 of the 570 tornadoes, occurring in the period 2000-2018, were of category EF1, thus 35 events were not considered for limited information on the time of occurrence.

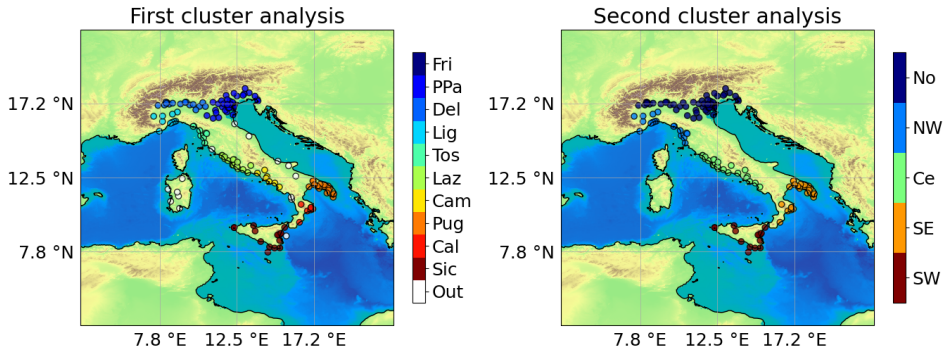

Figure 1: Cluster analyses based on location (left panel) and dynamical similarity (right panel). Coloured dots indicate tornado locations.

increase the population of each, we decided to merge up those clusters showing a high degree of *dynamical similarity*. To do so, we compared the cluster average mean sea level pressures by building a Pearson's correlation (pseudo-) distance matrix δ, that is

$$\delta_{ab} = 1 - \rho_{ab}, \quad \text{for any pair of clusters } a, b,$$

where ρ_{ab} indicates the Pearson's correlation coefficient between the cluster average mean sea level pressures relative to a and b. We merged neighbouring clusters having $\delta < 0.3$ (i.e. linear correlations higher than 70%), discarding outliers. The new family of 5 clusters, shown in Figure 1, right panel, included:

1. SW, the Sicily cluster, composed by 13 events;
2. SE, the South-East cluster (over Ionian Calabria and Puglia), composed by 23 events;

3. Ce, the Center cluster (over Campania and Lazio), composed by 23 events;
4. NW, the North-West cluster (over Tuscany and Liguria), composed by 17 events;
5. No, the North cluster (over Piedmont, Lombardy, Emilia-Romagna, Veneto and Friuli-Venezia Giulia), composed by 51 events.

It is worth noting that all the new clusters, but NW, were results of cluster merging with $\delta < 0.2$.

2.4. Calculation of mean states and standardised indices

For each cluster a we defined its *average state* as the fictitious state composed by mean atmospheric variables (see Equation 1 ahead). Furthermore, for any such mean variable, we defined its anomaly and standardised index (SI), computed with respect to the relative cluster composite climatology (equations 2 and 3 respectively):

$$av_a(x) = \frac{1}{\text{number of events in } a} \sum_{\text{events in } a} x_{\text{event}}, \tag{1}$$

$$an_a(x) = av_a(x) - clim_a(x), \tag{2}$$

$$ind_a(x) = \frac{an_a(x)}{std\_clim_a(x)}, \tag{3}$$

where x is the variable (e.g. temperature, specific humidity etc.) and $clim_a(x)$ and $std\_clim_a(x)$ are the climatological mean and the standard deviation, respectively. The climatological fields were computed considering all the data for each of the 19 years of the reanalysis dataset within ±1 hour and within ±1 day from the event time, finally adjusted to exclude any (known) tornadic event in the adjacent 3 hours in this time windows. Each sample includes up to $170 = 19 \times 3 \times 3 - 1$ (years × days × hours minus one to account for the event itself) timesteps.

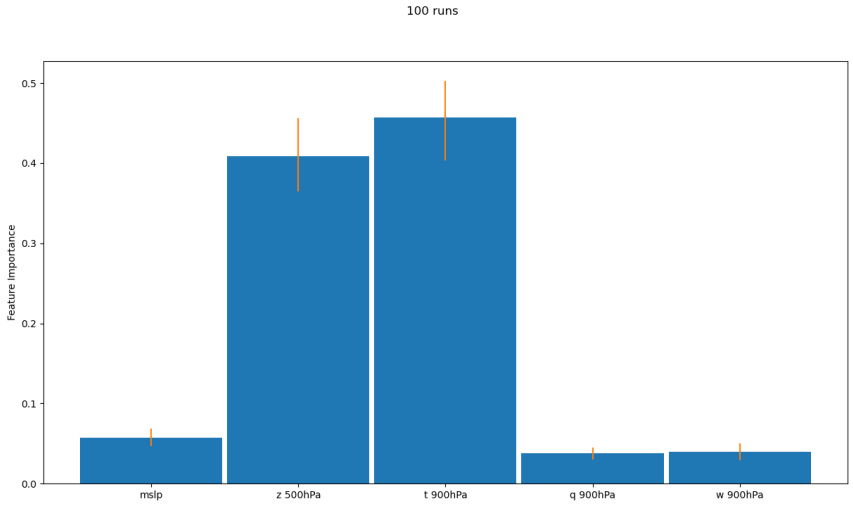

Figure 2: Feature importances over 100 Random Forests. Blue bars and orange lines indicate mean values and confidence intervals (5^{th}-95^{th} percentiles) respectively.

3. Results

3.1. Mean synoptic fields

In this study we aim to identify specific synoptic patterns of atmospheric variables, such as pressure fields, humidity and temperature associated to tornado occurrences in Italy. To select the pressure levels in which the chosen variables show the greatest variability we adopted a statistical criterion. Precisely, we built several random forests (RFs) (Breiman (2001)) ingesting the synoptic fields, with the scope of determining those displaying the most characteristic patterns (i.e. anomalous with respect to standard conditions).

We chose to compare five different synoptic variables, namely the mean sea level pressure ($mslp$), geopotential height (z), temperature (t), specific humidity (q) and vertical wind (w). For each parameter (but $mslp$) we trained 100 RFs

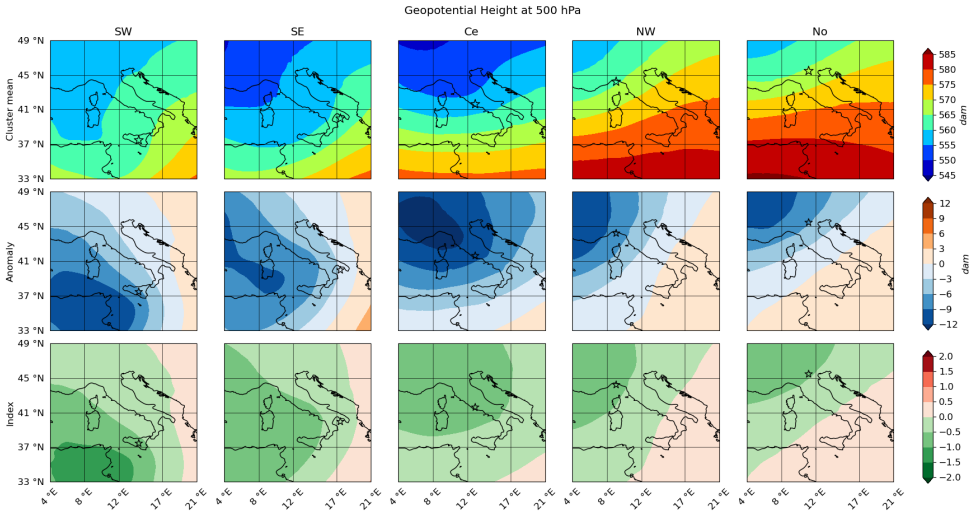

Figure 3: Cluster geopotential height at 500 *hPa*. For each cluster (columns) we computed the average geopotential height at 500 *hPa* (first row), its anomaly (second row) and standardised index (third row). Anomaly and index are computed with respect to the composite climatology. Black stars indicate the mean tornado coordinates.

to identify the most relevant pressure levels, namely those characterised by the most discriminating patterns (see Appendix A for details). Then, we trained an additional RF ensemble fed with the above variables at the selected pressure levels (500 *hPa* for z and 900 *hPa* for t, q and w). As summarized in Figure 2, the 500 *hPa* geopotential height and the low-level temperature turned out to be the most relevant features identifying the tornado-related synoptic patterns, followed by the mean sea level pressure and, marginally, by the low-level specific humidity and vertical wind.

3.1.1. Geopotential Height

Figure 3 shows the geopotential height at 500 *hPa* for each cluster in terms of mean state, anomaly and SI. It is shown that, in clusters SW, SE and Ce a

prominent trough wedges into the central Mediterranean Sea (more elongated in the former two). On average, tornadoes occur on the eastern side of the trough, close to the axis, in a region of southwesterly currents for SW and SE, while the flow appears zonal for Ce. Remarkably, in SE, tornadoes occur in the transition zone between the trough and the ridge. In NW and No a diffluent trough penetrates in the Mediterranean only marginally, as the minimum remains confined over central/northern Europe.

Negative anomalies are associated with the trough, deeper than -9 *dam* nearby the average tornado location in all cluster but SE, where the anomaly is weaker. On average, tornadoes occur on the south-eastern side of the maximum anomaly for Ce, NW and No, on the north-eastern side for SW, while for SE the tornadoes are located in an area of weak negative anomaly east of the maximum anomaly.

The configuration of the SI is similar to that of the anomaly for each cluster; cluster SW shows the deepest anomaly, located over North Africa, of less than -1.0.

3.1.2. Mean Sea Level Pressure

The mean state of each cluster shows a mean sea level pressure minimum lying generally nearby the mean tornado location, as shown in Figure 4.

In clusters SW, SE and Ce the mean tornado locations are East of the *mslp* minima, in an area of maximum pressure gradient. The locations of the minima change among the clusters: between Sicily, Sardinia and Tunisia in SW, over the Tyrrhenian Sea between Sardinia and central Italy in SE (thus, several hundreds *km* far from the average tornado location), over an extensive area from the Ligurian Sea to the eastern Po valley and the northern Adriatic in Ce (the latter feature may be indicative of some variability in the location of the minimum in the single

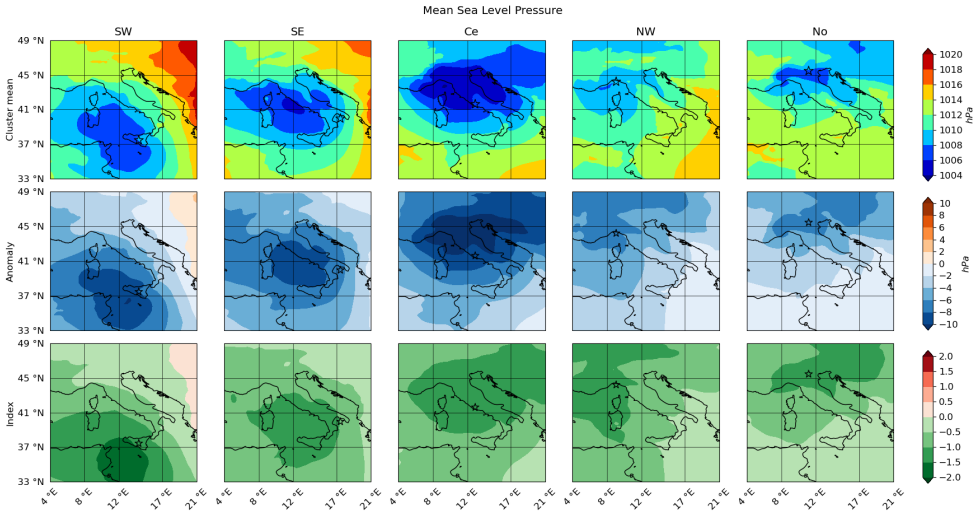

Figure 4: Cluster mean sea level pressure. For each cluster (columns) we computed the average mean sea level pressure (first row), its anomaly (second row) and normalized index (third row). Anomaly and index are computed with respect to the composite climatology. Black stars indicate the mean tornadoes coordinates.

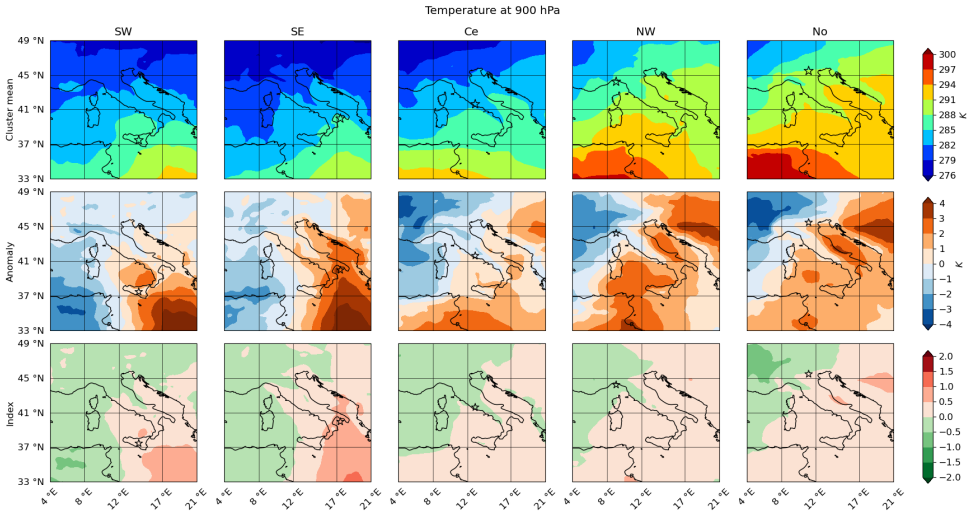

Figure 5: Cluster temperature at 900 *hPa*. For each cluster (columns) we computed the average temperature at 900 *hPa* (first row), its anomaly (second row) and normalized index (third row). Anomaly and index are computed with respect to the composite climatology. Black stars indicate the mean tornadoes coordinates.

case). Differently, in clusters NW and No, the pressure minima and the mean tornado locations are very close (the minima are located in the Gulf of Genoa and in the Po valley, respectively).

3.1.3. 900 hPa Temperature

The average 900 *hPa* temperature field of each cluster is shown in Figure 5. Clusters SW and SE are characterized by a warm anomaly over the Ionian Sea, extending northward from Libya, whose northernmost tip (with anomaly above $3°C$ and SI above 0.5) approaches Apulia region (SE cluster). As discussed in Miglietta et al. (2017a) for an EF3 case over the Ionian region, the tornado developed when the northern end of the warm tongue was advected toward an area of strong low-level shear (see later). Also, in SW and SE clusters, a weaker cold anomaly

(SI below -1) extends southward to Algeria and Tunisia, due to the northerly flow associated with the cyclonic circulation (see Figure 4).

In cluster Ce, in contrast, a weak warm anomaly (in absolute and relative terms) develop over southern and central Italy, while a cold anomaly extends to Sardinia and northern Italy, but the intensity of these anomalies in terms of SI are rather small.

The northern clusters NW and No, in turn, show different patterns. The high absolute values in the southern Mediterranean suggest that these cases occur mainly during summer (Miglietta and Matsangouras, 2018). For cluster NW, tornadoes occur in the presence of a cold anomaly entering the Po valley from the North-West, and reaching on its southern side the Ligurian sea and Tuscany. The values of this anomaly over the Italian regions is relatively small, in particular in terms of SI. Cluster No is characterised by a colder anomaly North-West of the Alps; due to the orographic blocking, the cold-air enters only marginally the Po valley, on its western side, and produces a small negative anomaly in the Prealps. In contrast, a warm anomaly still lies above the Adriatic Sea, so that the mean tornado location is nearby the border between air masses of different characteristics.

It is worth noting that, in all cases, tornadoes develop in a region of 900 hPa temperature between $12°C$ and $15°C$.

3.1.4. 900 hPa Specific humidity

The 900 hPa specific humidity field shows high values in the areas affected by tornadoes, in particular in clusters No and NW (specific humidity is above 9 $g \cdot kg^{-1}$ in Tuscany and northern Italy, and in the northern Adriatic, respectively).

However, in term of absolute anomaly and SI, the specific humidity in clusters SW and SE show higher values over a wide area (above 2 $g \cdot kg^{-1}$ and above

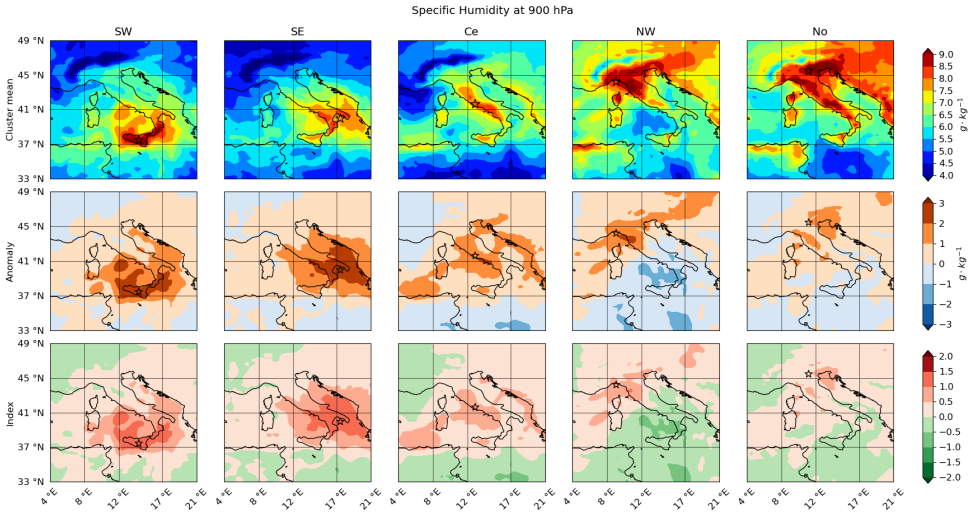

Figure 6: Cluster specific humidity. For each cluster (columns) we computed the average specific humidity (first row), its anomaly (second row) and normalized index (third row). Anomaly and index are computed with respect to the composite climatology. Black stars indicate the mean tornadoes coordinates.

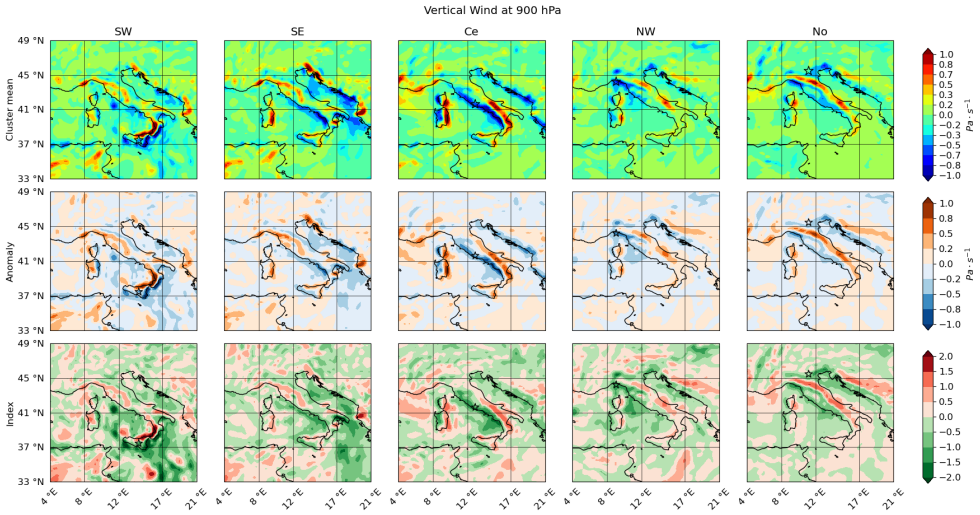

Figure 7: Cluster vertical wind at 900 *hPa*. For each cluster (columns) we computed the average vertical wind at 900 *hPa* (first row), its anomaly (second row) and normalized index (third row). Anomaly and index are computed with respect to the composite climatology. Black stars indicate the mean tornadoes coordinates.

1.0, respectively). The high values of humidity and the small departure from climatology in No are indicative of the summer occurrence of tornadoes in this cluster.

3.1.5. 900 hPa Vertical wind

Average low-level vertical winds (Figure 7) are indicative of a mesoscale environment favorable to ascending motion (negative values) in the areas of tornado occurrences. For all cluster, but SE, this feature seems related to the orographic uplift induced by the low-level wind circulation inferred from the pressure fields (Figures 3 and 4), on the upstream side of the Alps and the Appenines. Nearby the event sites, negative values are observed in terms of absolute anomalies and SI (the latter generally below -1). Notably, the vertical motion in SW seems to be re-

lated to a mesoscale feature over the northern Ionian Sea, rather than to orographic forcing.

3.2. Mesoscale precursors

Among the most robust diagnostic atmospheric variables associated to tornadoes, as recalled in §1, we consider here: WS, CAPE, SRH and LCL.

Because of the lack of extensive samples for some clusters, we decided to regroup all events in two classes, based on their intensity (EF1 or EF2+). Then, for each class, we evaluated the SI values of both WS and SRH at various pressure levels as reported in Figure 8. In that figure each violin represents the probability density function (pdf) of a given distribution. Any such pdf, which has been smoothed by convolution with a gaussian kernel, is oriented and reflected along the vertical line. The internal white boxes within are standard box-plots highlighting the 5th and 95th (whiskers), the interquartile range (boxes) and the median (black dots).. The comparison among LLS, MLS and DLS revealed that LLS turned out to be the precursor showing the largest departure from the climatology, hence the $900\,hPa$ level was chosen for wind shear. The SI median and 95th percentile of $\mathrm{SRH}_{900\,hPa}$ resulted slightly larger than that of $\mathrm{SRH}_{700\,hPa}$. Consequently, $\mathrm{SRH}_{900\,hPa}$ was preferred to $\mathrm{SRH}_{700\,hPa}$ for the analysis.

The variable and SI distributions or LLS, CAPE, $\mathrm{SRH}_{900\,hPa}$, LCL are shown in the violin plots of Figure 9. The distributions of the potential precursors showed that EF2+ events are generally associated with more extreme SI values than EF1. In terms of real values, instead, the differences between the two classes are less clear, but EF2+ tornadoes generally show slightly larger values than EF1 in terms of medians and percentiles. For example, although EF1 tornadoes have higher extreme values of LLS (greater than 15 $m \cdot s^{-1}$), the EF2+ median is equal to

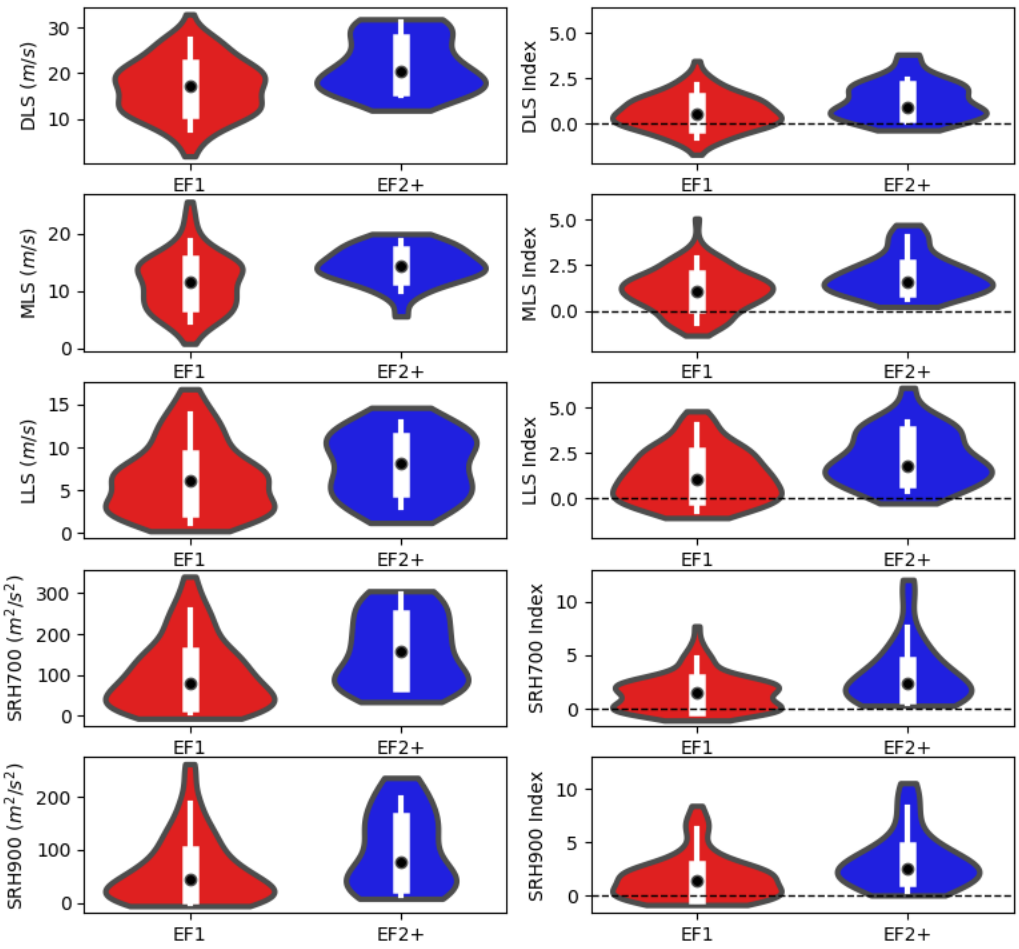

Figure 8: Distributions of real values of mesoscale precursors (left panels) and standardized indices (right panels) of DLS, MLS, LLS and SRH at 700 hPa and 900 hPa (EF1 red violins, EF2+ blue violins). Black dots indicate the median, white boxes bound the interquartile range and the whiskers extend up to the 5th and the 95th percentiles.

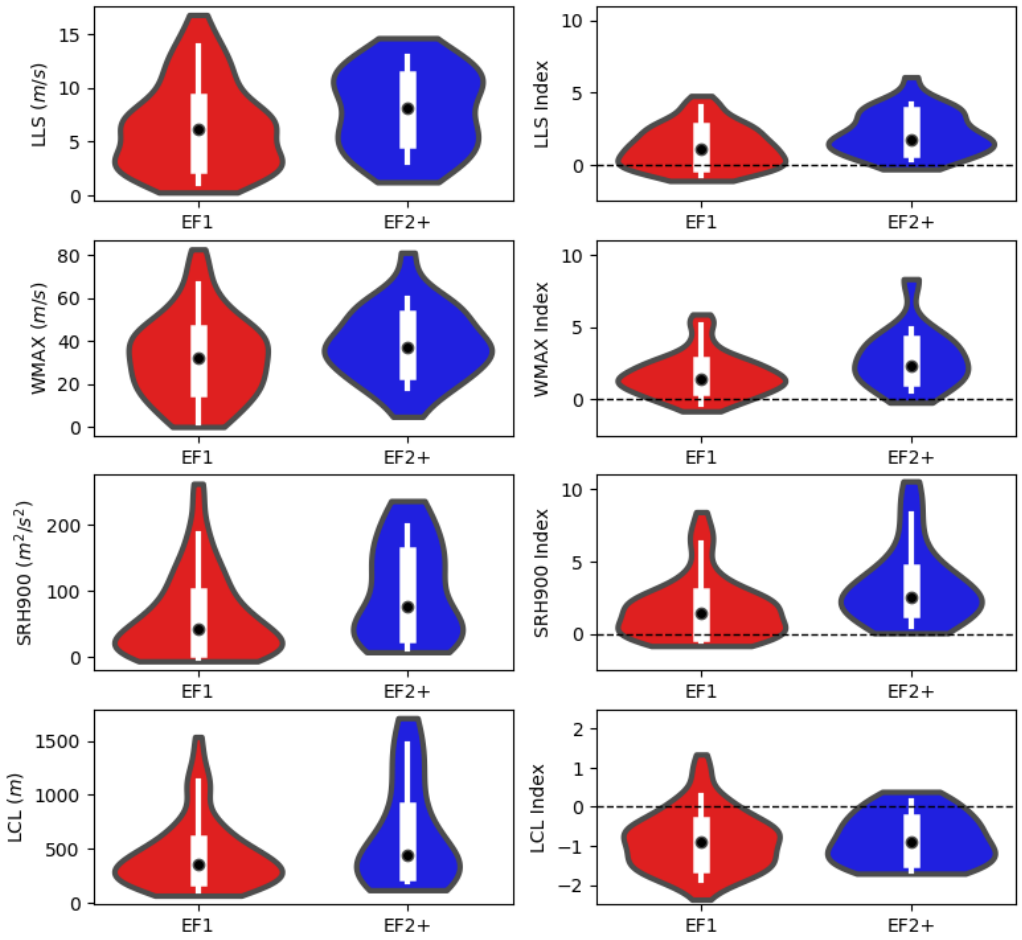

Figure 9: Distributions of mesoscale precursors (left panels) and standardized indices (right panels) of low-level wind shear LLS, maximum updraft velocity WMAX, 1000 - 750 *hPa* storm relative helicity and lifting condensation level LCL per tornado category (EF1 red violins, EF2+ blue violins). Black dots indicate the median, white boxes bound the interquartile range and the whiskers extend up to the 5th and the 95th percentiles.

(a) EF1

Variable	5th	Median	95th
LLS	1.1	6.1	13.9
$SRH_{900\,hPa}$	-0.5	43.5	187.5
WMAX	1.8	31.7	67.1
LCL	109	358	1139

(b) EF2+

Variable	5th	Median	95th
LLS	2.5	8.2	13.1
$SRH_{900\,hPa}$	12.2	76	214.5
WMAX	15.1	36.9	61.3
LCL	174	438	1559

Table 1: Mesoscale precursors statistics for EF1 (a) and EF2+ (b) tornadoes in terms of their medians and 5th and 95th percentiles. Units: $m \cdot s^{-1}$ for LLS and WMAX, $m^2 \cdot s^{-2}$ for SRH and m for LCL.

8.1 $m \cdot s^{-1}$, about 2 $m \cdot s^{-1}$ higher than the EF1 category (Table 1). Regarding the SI, for LLS, WMAX and $SRH_{900\,hPa}$, EF2+ indices are greater than 0 (above the mean climate conditions), except for some outliers in the WMAX and LLS distributions (Figure 9). In particular, for WMAX and $SRH_{900\,hPa}$, values over the 75th percentile, are greater than 4, revealing very strong index anomalies for almost 25% of the events. For EF2+ tornadoes, the medians of SIs are 1.7 for LLS and 2.4 for WMAX and 2.5 for SRH, i.e. much higher than the average climate (Table 2). Regarding EF1 tornadoes, anomalies turn out to be less pronounced, but still relevant (median values above 1), although about 25% of the cases are below the climatology. For LCL, the absolute index values are generally smaller than for the other variables, with a median around -0.9 and extreme values close to -2 for EF1 tornadoes (slightly higher than EF2+). However, more than 75% of LCL index values are below the climatologic value (Figure 9).

(a) EF1

Variable	5th	Median	95th
LLS	-0.7	1.1	4.1
$SRH_{900\,hPa}$	-0.5	1.5	6.4
WMAX	-0.3	1.4	5.2
LCL*	0.4	-0.9	-1.9

(b) EF2+

Variable	5th	Median	95th
LLS	**0.3**	1.7	4.2
$SRH_{900\,hPa}$	**0.3**	2.5	8.9
WMAX	**0.4**	2.4	6.7
LCL*	0.2	-0.9	-1.7

Table 2: SI statistics per variable for EF1 (a) and EF2+ (b) tornadoes. Values in bold correspond to 5^{th} percentiles of SI distributions far away above zero. *For LCL, which has negative mean SI, the 5^{th} and 95^{th} percentiles have been reversed (e.g., 95th percetile refers to the value farther from 0).

The previous analysis has shown that extreme values of CAPE, low-level WS, mid-level SRH and LCL are frequently associated with tornadic activity. It is then natural to ask which mesoscale patterns of these variables are associated with tornado occurrences. To satisfy this curiosity we analysed their mean fields and the relative statistics similarly as §3.1. Moreover, in order to ensure/guarantee the relevance of these statistics, we applied a statistical test aiming to establish their significance (see Appendix B for details). It turned out that all the highest anomalies occurring nearby the mean tornado sites were, indeed, significant.

3.2.1. Low-level Wind Shear

Higher values of LLS are reported in SW and SE areas. This pattern reflects the anomaly and index configuration, with higher values of LLS over the Ionian Sea for cluster SE, and over the Ionian and the southern Tyrrhenian seas for cluster SW (Figure 10).

The mean LLS turns out to be strongly coherent among clusters, since the

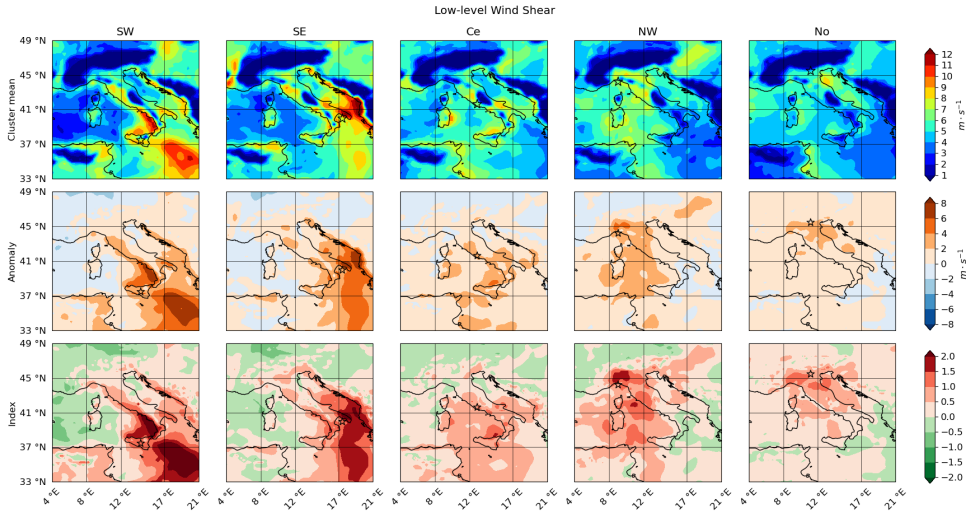

Figure 10: Cluster LLS. For each cluster (columns) we computed the average wind shear from the surface to 900 *hPa* (first row), its anomaly (second row) and normalized index (third row). Anomaly and index are computed with respect to the composite climatology. Black stars indicate the mean tornadoes coordinates.

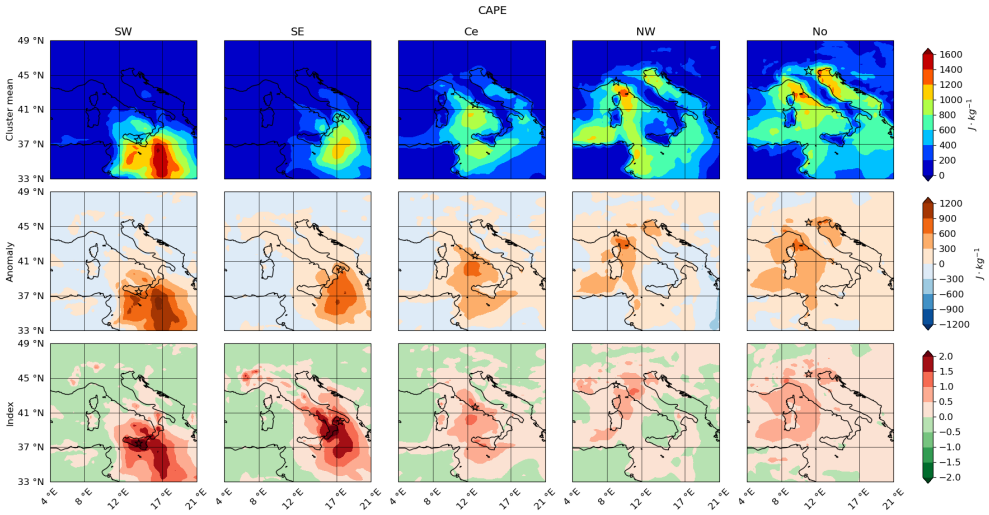

Figure 11: Cluster CAPE. For each cluster (columns) we computed the average CAPE (first row), its anomaly (second row) and normalized index (third row). Anomaly and index are computed with respect to the composite climatology. Black stars identify the mean tornadoes coordinates.

maximum positive anomalies (above $2\,m \cdot s^{-1}$) occur in the neighbourhood of the mean tornado occurrence in all cases. The strongest signal comes from the southern clusters where indices become highly relevant, with values above 2 (anomalies above 6 $m \cdot s^{-1}$); however, also in the other clusters, the values are greater than 1 near the tornado location.

3.2.2. CAPE

CAPE patterns highlight areas of potential instability, which surround the mean tornado location of each cluster (Figure 11). The highest values are found in cluster SW, where a wide area over the Ionian Sea, pretty close to the tornado mean locations, shows values above $1600\,J \cdot kg^{-1}$.

The strongest anomaly is for cluster SW (about $1200\,J \cdot kg^{-1}$), while the lowest anomaly (about $600\,J \cdot kg^{-1}$) occurs for No. However, considering SI, the most

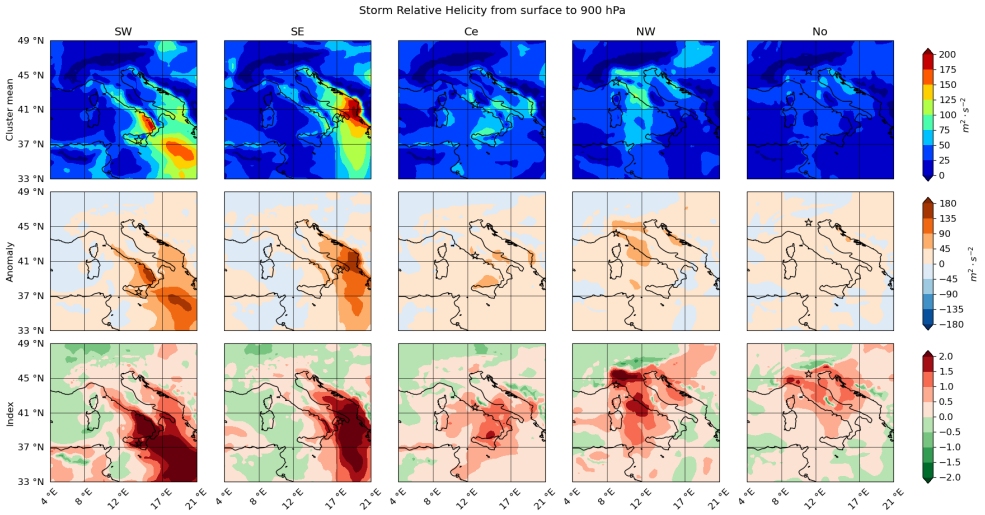

Figure 12: Cluster storm relative helicity. For each cluster (columns) we computed the average storm relative helicity from the ground to 900 *hPa* (first row), its anomaly (second row) and normalized index (third row). Anomaly and index are computed with respect to the composite climatology. Black stars indicate the mean tornadoes coordinates.

relevant departures from climatology are shown by SW and SE, which are characterized by indices above 2.0, whereas the peak for the other clusters are generally around 1.0. Although the CAPE values in cluster No are among the highest, the anomaly is not extreme, since high values of CAPE can be frequently observed during summer, when these events mostly occur (Miglietta and Matsangouras, 2018).

3.2.3. Storm Relative Helicity

The highest values of the 1000-900 *hPa* storm relative helicity occur for the two southern clusters, as observed for CAPE and WS, with values close to 200 $m^2 \cdot s^{-2}$ in cluster SE (Figure 12). In contrast, the value of SRH for the other clusters is smaller, in particular for No where SRH is less than 75 $m^2 \cdot s^{-2}$ nearby

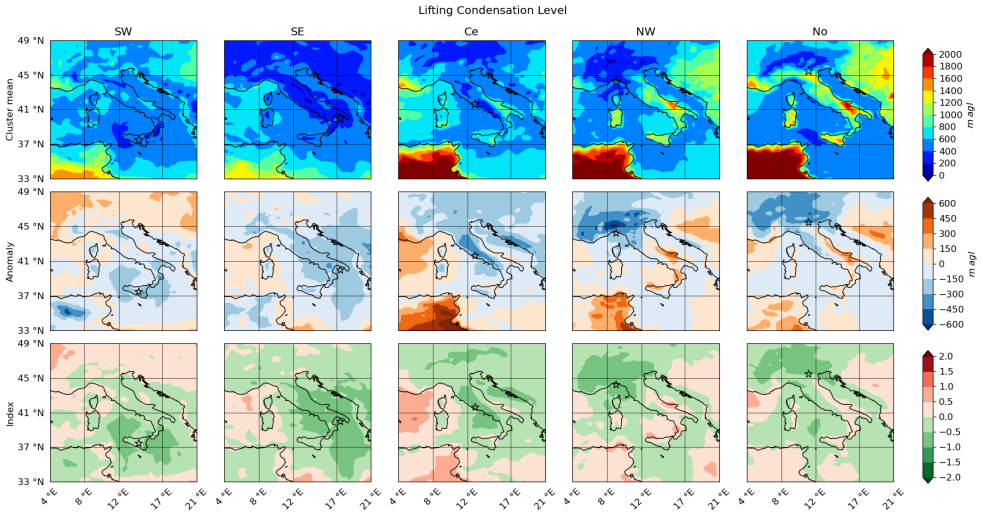

Figure 13: Cluster lifting condensation level. For each cluster (columns) we computed the average lifting condensation level (first row), its anomaly (second row) and normalized index (third row). Anomaly and index are computed with respect to the composite climatology. Black stars indicate the mean tornadoes coordinates.

the mean tornado location. Anyway, positive anomaly and SI characterise all clusters. Cluster SW, SE and NW, however, show larger anomalies and greater departures from climatology, as SI is above 2.0 in extensive areas.

3.2.4. LCL

LCL is below the climatological values in all clusters. The anomalies are lower (in absolute value) in the southern clusters, while the values of SI are comparable (between -0.5 and -1.0) in all clusters (Figure 13). In cluster No, the tornado location is at the border between anomalies of different sign, North of an area of positive anomaly on the southern part of the North Adriatic Italian coast.

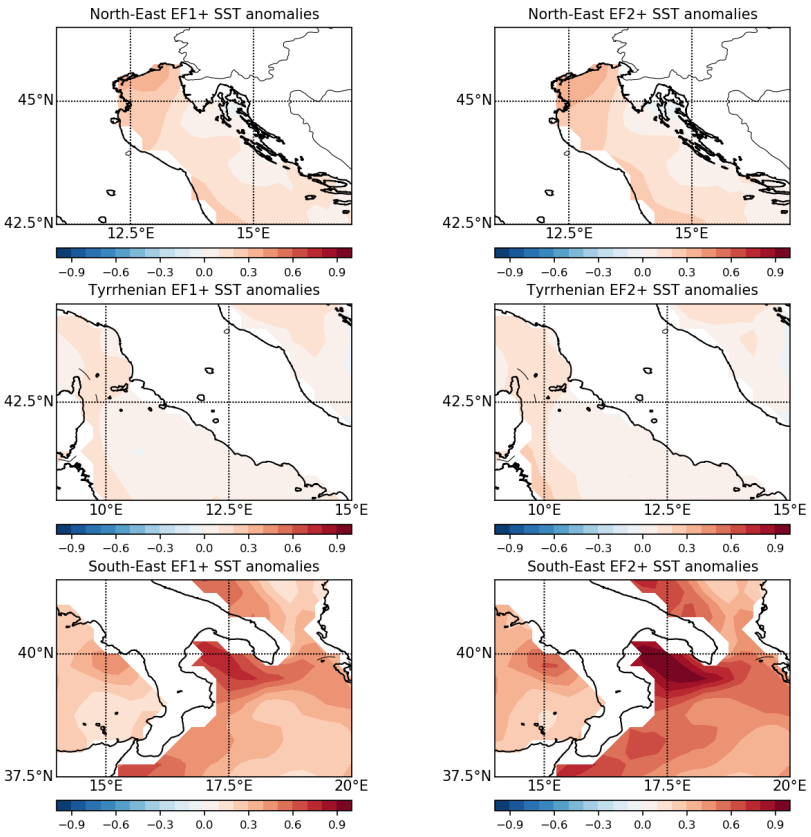

Figure 14: SST anomaly maps regarding three main coastal areas where tornadoes occurred. Top North-East, Middle) Tyrrhenian, Bottom) South-East. In the column on the left are present maps relative to EF1+ tornadoes, on the right to EF2+

3.3. Sea Surface Temperature

A non-atmospheric parameter, SST, deserves a separate discussion. Miglietta et al. (2017b) showed significant changes in supercell updraft helicity and vertical

velocity associated with relative small variations of SST for a tornado over the Ionian coast of Apulia region.

They suggested that a positive SST anomaly may favour supercell formation and intensification originated as a waterspout over the Mediterranean region for tornadoes of similar origin and evolution. Moreover, Marín et al. (2020) found an increase in the atmospheric instability impacting the storm severity related to small SST increases during tornadoes in south-central Chile. To investigate this speculation we seized the opportunity of this study, involving a large number of coastal tornadoes, in order to analyse the average SST anomalies in different coastal sub-regions.

Because of the lack of a significant number of coastal tornadoes for each cluster, we decided to merge together the tornadoes along the Ionian coast in cluster SW and SE, those in clusters Ce and NW (along the central and northern Tyrrhenian coast), and to finally consider the coastal tornadoes in No (along the northern Adriatic). All coastal tornadoes were considered, included those originated just inland, supposing the air-sea interaction may have modified the characteristics of the air mass before reaching the region of tornadogenesis. Thus, three wider sub-regions were created and the SST anomaly was calculated for each of them. We obtained 31 EF1+ and 7 EF2+ tornadoes for the north-eastern sub-region, 40 EF1+ tornadoes and 6 EF+ tornadoes for the Thyrrhenian sub-region, 23 EF1+ and 8 EF2+ tornadoes for the southern area. In Figure 14, maps of SST anomaly relative to EF1+ and EF2+ tornadoes (left and right column respectively), for the three main sub-regions (North-East, Tyrrhenian, South-East), are shown. Regarding the southern sub-region, a positive anomaly of more than $0.7^\circ C$ (over $0.9^\circ C$ for EF2+ tornadoes) is present in the northern Ionian Sea, in agreement with the

results of Miglietta et al. (2017b). This result suggests that SST positive anomalies may play a significant role in the formation of tornadoes in this sub-region. A warm SST anomaly, of about $0.4° - 0.5° C$, characterises the north-eastern sub-region as well, with small differences between the two categories of tornado intensity. Differently, for the Thyrrhenian area no relevant SST anomalies are found (of about $0.2° C$), suggesting a limited impact of air-sea interaction processes in the development of these tornadoes.

4. Discussion

We have seen in the previous sections that each cluster is characterised by some peculiar characteristics; however, similar configurations have been detected as well. Each mean state displays a geopotential minimum in the mid-troposphere, over the north-western side of the mean tornado locations (Figure 3), indicating the approach of a synoptic trough from the West. The configuration of the mean sea level pressure, which is shifted to the south-eastern side with respect to the upper-level depression (Figure 4), suggests that the structure is far from occlusion, still in a phase of development.

If the baric configurations show similar patterns for all clusters, the same is not true for the $900\,hPa$ temperature. In southern clusters, tornado locations are characterised by a warm air intrusion from the South, whereas in northern clusters they are affected by a cold air intrusion from the North-West. The warm intrusion in the southern clusters is associated with the cyclonic circulation due to the pressure configuration, which determines strong southerly winds from northern Africa. In contrast, the mean sea level pressure minimum of northern clusters is centered at the tornado mean sites and it is the high-level depression that brings

upper-level colder air from continental Europe, increasing the potential instability. The dynamics in cluster Ce are less clear: relevant anomalies are confined far away from the location of this cluster. Figures 3 and 4 suggest that in cluster Ce low-level winds are south-westerly, thus nearly orthogonal to the main coastline. The change in roughness for parcels moving from sea to land affects the low-level wind field near the coast, favouring the generation of convergence lines, which are known to be a genesis mechanism for non-mesocyclonic tornadoes. Also, the south-westerly winds move over rather uniform low level temperatures (Figure 5), and are not associated with significant advection. In conclusion, considering also the relatively lower values (compared to the other clusters) of the mesoscale precursors in terms of anomalies and SI one may suppose that different dynamics develop for Ce tornadoes compared to other clusters. However, this point needs further investigations in future studies.

A different behaviour is also detected for specific humidity (Figure 6), which shows larger absolute values in the northern regions, but higher anomalies and indices over the central and southern regions. For central and southern clusters the mean winds come from the open sea, thus it is very likely that the incoming air has increased its water content by ventilation. Differently, the fetch in northern regions is much shorter, due to the land distribution. In these regions, tornadoes occur mainly during summer (Miglietta and Matsangouras, 2018), thus the accumulation of humidity in the low levels is due to the strong evaporation from sea, rivers and lakes. In all cases the presence of high humidity content leads to increased potential instability.

One may conclude that the main ingredients for tornado occurrence in southern Italy are the presence of severe wind (shear) and moderate humidity content,

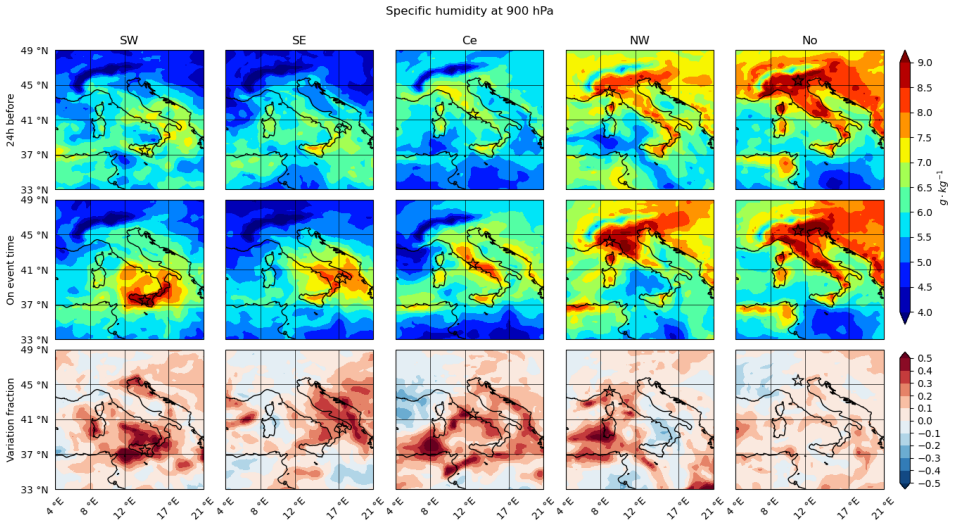

Figure 15: 900 hPa specific humidity 24 hour differences. Cluster mean variable 24 hour before the event (first row), on event time (second row) and the relative incremental fraction (third row).

gained by the air mass during its movement over the Mediterranean Sea. In the northern cases, instability is triggered by the arrival of colder air over the Po Valley in the mid-troposphere over very warm and moist low-levels, where humidity is generated by the strong evaporation typical of the season of occurrence (summer). The latter point is also confirmed by the comparison with the humidity maps 24 hours before the tornado events (Figure 15). It can be seen that, in northern regions, high humidity values were already present one day before the tornado occurrences, as a consequence of the evaporation of water bodies during the dry/hot season. Differently, southern and central regions are mainly affected by moist advection causing a 50% increase of local specific humidity in 24 hours.

5. Conclusions

In this study we analysed the synoptic configurations and the large-scale variation of relevant mesoscale tornado precursors associated to tornado occurrences in the Italian peninsula. We based our study on the dataset validated in Miglietta and Matsangouras (2018) and extended by Ingrosso et al. (2020), considering tornadoes occurred between 2000 and 2018. To highlight the most relevant anomalies, we selected only the events of EF category greater or equal to 1 and recorded with high temporal accuracy. The chosen set, composed by 149 distinct events, was further divided into 5 clusters by considering the geographical location and the degree of dynamical similarity, the latter being based on the mean sea level pressure synoptic configuration. Each cluster resulted to be representative of a specific geographical region: namely southeastern Italy, Sicily, central Tyrrhenian coast, northern Tyrrhenian coast and northern Italy/Po valley.

The analysed environmental variables were the geopotential height, mean sea level pressure, temperature, specific humidity, vertical wind component, vertical wind shear, CAPE, storm relative helicity, lifting condensation level and, for coastal tornadoes only, the sea-surface temperature. Each variable was averaged over the cluster elements to produce a mean atmospheric state representative of a given cluster. In addition, we compared such typical states with their climatological means, thus obtaining both quantitative and qualitative estimates of their anomaly/exceptionality with respect to the mean climate. We identified specific synoptic configurations favourable to tornadogenesis in the considered regions. The analysis of relevant mesoscale tornado precursors, such as the storm relative helicity, confirmed the triggering potential of these large-scale configurations.

Remarkably, high SST anomalies in the Ionian Sea were related with southern

coastal tornadoes, in agreement with Miglietta et al. (2017b) who proved that ocean heat fluxes may intensify updraft helicity and vertical velocity in a EF3-tornado spawning supercell. For SE tornadoes, the main mean sea level pressure disturbance is several hundred *km* far from the average tornado location. In fact, the tornadoes occur when the northern end of a warm/moist tongue is advected toward an area of strong low-level shear. In contrast, in northern regions, the combination of high humidity content due to evaporation, with cold-air intrusion from continental Europe was identified as peculiar driving mechanism related to tornado occurrences. Further investigations are necessary to better understand the role of SST for coastal tornadoes, especially considering its projected increase in the future climate simulations (Kirtman et al., 2013).

This study confirms the important role of some mesoscale parameters such as CAPE, wind shear, LCL an SRH for tornadoes over the Italian regions, as shown by the large anomalies and SI values over all the clusters. Further analyses are necessary in order to understand the possible different values of these anomalies between mesocyclonic and non-mesocyclonic tornadoes and between tornadic and non-tornadic thunderstorms.

Appendix A. Random Forest

Appendix A.1. Generalities

Random Forests are ensemble learning methods, where the model predictors are decision trees (see Haupt et al. (2009) for an overview of learning methods). In a RF, each tree is trained on a random sampling[3] of the entire dataset and the

[3]In this study we randomly sampled 80% of the whole dataset each time

model prediction is nothing else then the average prediction among trees.

During the training each tree is optimized as follows. At any step, if the arresting criteria (e.g. weak information gain, few samples left) are unsatisfied, a node is created and an input variable together with a threshold value are chosen to reduce a prescribed error function, or impurity, E, splitting the data accordingly with the variable and the threshold. For what concerns us, E has been chosen to be the Gini's impurity (or Gini's diversity index in Breiman et al. (1984)), which, at node n, is given by

$$E_n = 2p_n(1 - p_n),$$

where p_n is the fraction of tornadic events of the training data at node n.

Each tree represents a classification scheme where, at any node, the input observation is tested and passed to one of the next two child nodes, until a terminal node is reached and a prediction, about the probable class of the input observation, is made. Therefore, trees are usually adopted to make predictive analysis. However, due to their simple interpretation, they may be used to gain additional information. As we already said, at any node a single feature, chosen to reduce the node impurity, has been identified. Therefore, the cumulative weighted sum over the feature-related nodes of the impurity negative gradient, simply called *feature importance* (Breiman (2001)), gives a measure of the variable relevance, ranging from 0 to 1 accordingly with its relevance degree, in the classification scheme.

Appendix A.2. Set-up and training

The training dataset was built as follows. Firstly, for each tornado event, we randomly sampled 9 more states in its climatology to compose the class of non-tornadic events which, together with the class of tornadic events, defined a set of

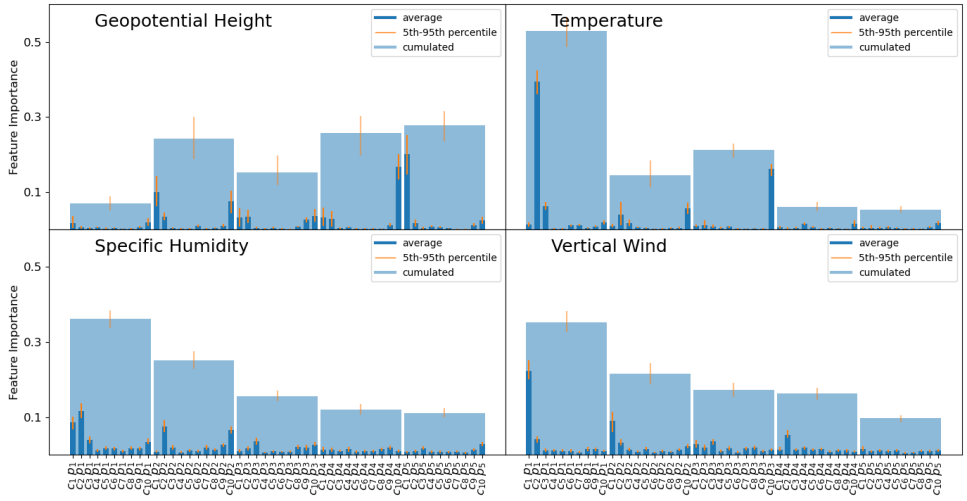

Figure A.16: Intra-species feature importances over 100 Random Forests. Blue bars and orange lines indicate mean values and confidence intervals (5^{th}-95^{th} percentiles) respectively. Here features are correlations of variable sections (at pressure levels $p_1 = 900, p_2 = 800, p_3 = 700, p_4 = 600, p_5 = 500\ hPa$) against principal components $(c_1, \ldots, c_{10})$. Summing over the components (light blue bars) gives the importance of a single variable section.

atmospheric states S[4]. Secondly, we chose 4 different types, or species, of variables: geopotential height (z), temperature (t), specific humidity (q) and vertical wind (w).

For each type x and sample s we took the sample-related variable sections x_{s,p_i} at prescribed pressure levels p_i of 900, 800, 700, 600 and 500 hPa. We denote this set by $S^{(x)}$.

Due to the large amount of data defining each $S^{(x)}$, we applied a dimensionality reduction by principal component analysis (PCA). Precisely, for each state s and each pressure level p_i, we computed the first 10 principal components of the variable x_{s,p_i} with respect to the full climatology of s, extracting the (absolute) coefficients of the decomposition. The reduced input space is denoted by $S^{(x)}_{10}$.

We trained 100 RF classifiers composed by 50 trees on each reduced input space, computing the features importance of each. To increase the sensibility of the models to tornadoes we re-balanced the dataset during the training by weighting the loss function. In this framework the features are correlations with the principal modes of the variable x at the various pressure levels, therefore the cumulative importance over all the components can be considered as the overall importance of that variable section (precisely, of its re-assembled copy) in the classification. It is worth noting that, at any run, each tree of the ensemble has been tested against the unseen part of the dataset to assess the model reliability.

We evaluated the mean Heidke's skill score hss (introduced in Heidke (1926) and known among statisticians as Cohen's κ from Cohen (1960)). This score takes

[4]We added more non-tornardic events with the aim of giving enough alternative configurations

values in $(-\infty, 1]$ as is given by

$$hss = \frac{acc - rnd}{1 - rnd},$$

where acc is the model accuracy (fraction of right predictions) and rnd is the probability of a random agreement between truth and prediction. By definition negative values of hss indicate no or weak agreement between predictions and observations, the zero value testifies that the model performances are good as those of a random model based only on the classes proportions whereas higher values indicate better performances. Obviously, a perfect classifier has $hss = 1$.

The models trained on z showed an hss with mean value 0.84 and a standard deviation of 0.01, those on t a mean of 0.77 and standard deviation of 0.02, those on q a mean of 0.37 and standard deviation of 0.02 and those on w a mean of 0.39 and standard deviation of 0.03.

It has to be noted that the models trained on z and t had higher performances. This could be due to the fact that their first 10 principal modes explained a high portion of the overall variability, values greater than 92%. On the contrary, the other variables were poorly represented, with their 10 modes explaining 60% (for q) or 40% (for w) of the entire variance.

Finally, after having identified the most relevant pressure levels for each variable (500 hPa for z and 900 hPa for the others, as shown in Figure A.16), we assembled a new reduced input dataset defined through the principal components of the single level variables and compared the extra-species importances (as already discussed in the text). We noted that, in this case, the average hss on the unseen data was 0.81 with a standard deviation of 0.16. The mean hss was lower for the model trained on z only, indicating the presence of relevant information in lower-level heights too.

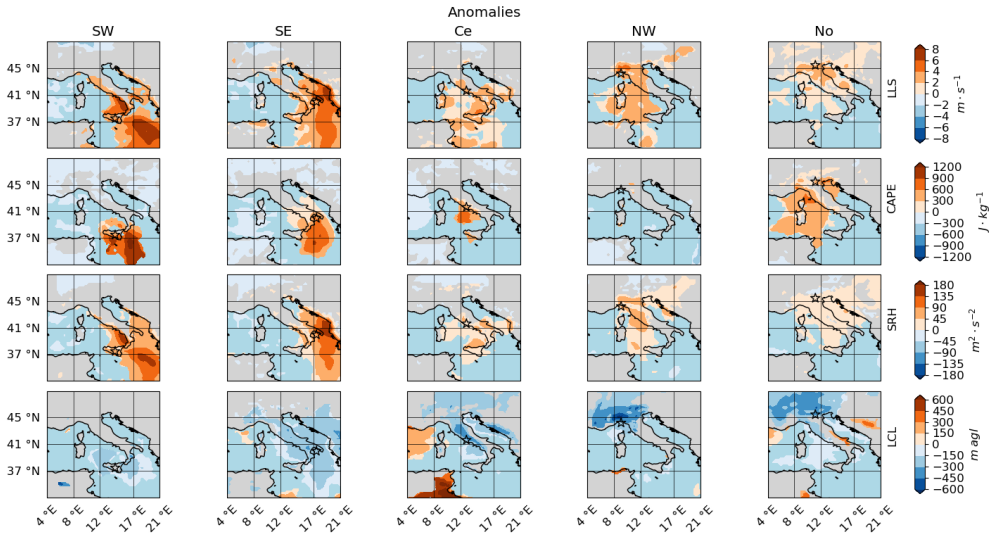

Figure B.17: Significant mean anomalies of LLS (first row), CAPE (second row), $\mathrm{SRH}_{900\,hPa}$ (third row) and LCL (fourth row) per cluster (columns). Only areas in which the mean cluster anomaly is different from zero with a significance level (Student's t-test) of 5% are shown.

Appendix B. Significance of precursors anomalies

To assess the relevance of the mesoscale precursors anomaly maps shown in §3.2, we performed a Student's t-test for each cluster. We rejected the null hypothesis of zero average anomaly with a significance level of 5%. Anomalies significantly different from zero are shown in Figure B.17.

References

Allen, J.T., Karoly, D.J., Mills, G.A., 2011. A severe thunderstorm climatology for australia and associated thunderstorm environments. Australian Meteorological and Oceanographic Society 61, 143–158. doi:10.22499/2.6103.001.

Breiman, L., 2001. Random forests. Machine Learning 45, 5–32.

Breiman, L., Friedman, J.H., Olshen, R.A., Stone, C.J., 1984. Classification and Regression Trees. Wadsworth and Brooks, Monterey, CA.

Brooks, H.E., 2009. Proximity soundings for severe convection for europe and the united states from reanalysis data. Atmospheric Research 93, 546 – 553. URL: http://www.sciencedirect.com/science/article/pii/S0169809508002858, doi:https://doi.org/10.1016/j.atmosres.2008.10.005. 4th European Conference on Severe Storms.

Brooks, H.E., 2013. Severe thunderstorms and climate change. Atmospheric Research 123, 129–138. doi:10.1016/j.atmosres.2012.04.002.

Brooks, H.E., Lee, J.W., Craven, J.P., 2003. The spatial distribution of severe thunderstorm and tornado environments from global reanalysis data. Atmospheric Research 67–68, 73–94. doi:10.1016/S0169-8095(03)00045-0.

Cohen, J., 1960. A coefficient of agreement for nominal scales. Educational and Psychological Measurement 20, 37–46.

Colquhoun, J.R., Shepherd, D.J., 1989. An objective basis for forecasting tornado intensity. Weather and Forecasting 5, 35–50. doi:10.1175/1520-0434(1989)004¡0035:AOBFFT¿2.0.CO;2.

Craven, J., Brooks, H., 2004. Baseline climatology of sounding derived parameters associated with deep, moist convection. Natl. Wea. Dig. 28, 13–24.

Davies, J.M., Johns, R.H., 1993. Some Wind and Instability Parameters Associated With Strong And Violent Tornadoes: 1. Wind Shear And Helicity. American Geophysical Union (AGU). pp. 573–582. doi:10.1029/GM079p0573.

Davies-Jones, R., 1984. Streamwise Vorticity: The Origin of Updraft Rotation in Supercell Storms. Journal of the Atmospheric Sciences 41, 2991–3006. doi:10.1175/1520-0469(1984)041¡2991:SVTOOU¿2.0.CO;2.

Doswell, C.A., Rasmussen, E.N., 1994. The Effect of Neglecting the Virtual Temperature Correction on CAPE Calculations. Weather and Forecasting 9, 625–629. doi:10.1175/1520-0434(1994)009¡0625:TEONTV¿2.0.CO;2.

Dupilka, M.L., Reuter, G.W., 2006. Forecasting tornadic thunderstorm potential in alberta using environmental sounding data. part i: Wind shear and buoyancy. Weather and Forecasting 21, 325–335. doi:10.1175/WAF921.1.

Emanuel, K.A., 1994. Atmospheric Convection. Oxford University Press.

Fujita, T.T., 1971. Proposed characterization of tornadoes and hurricanes by area and intensity. Satellite and Mesometeorology Research Project 91, 42 pp.

Giaiotti, D.B., Giovannoni, M., Pucillo, A., Stel, F., 2007. The climatology of tornadoes and waterspouts in italy. Atmospheric Research 83, 534–541. doi:10.1016/j.atmosres.2005.10.020.

Gianfreda, F., Miglietta, M., Sansò, P., 2005. Tornadoes in southern apulia (italy). Nat Hazards 34, 71—-89. doi:10.1007/s11069-004-1966-3.

Grams, J.S., Thompson, R.L., Snively, D.V., Prentice, J., Hodges, G.M., Reames, L.J., 2012. A climatology and comparison of parameters for significant tornado events in the united states. Weather and Forecasting 27, 106–123. doi:10.1175/WAF-D-11-00008.1.

Groenemeijer, P., van Delden, A., 2007. Sounding-derived parameters associated with large hail and tornadoes in the netherlands. Atmospheric Research 83, 473–487. doi:10.1016/j.atmosres.2005.08.006.

Grünwald, S., Brooks, H., 2011. Relationship between sounding derived parameters and the strength of tornadoes in europe and the usa from reanalysis data. Atmospheric Research 100, 479–488. doi:https://doi.org/10.1016/j.atmosres.2010.11.011.

Haupt, S., A., P., Marzban, C., 2009. Artificial Intelligence Methods in the Environmental Sciences. Springer.

Heidke, P., 1926. Berechnung des erfolges und der güte der windstärkevorhersagen im sturmwarnungsdienst. Geografiska Annaler 8, 301–349.

Hersbach, H., Bell, B., Berrisford, P., Hirahara, S., Horányi, A., Muñoz-Sabater, J., Nicolas, J., Peubey, C., Radu, R., Schepers, D., Simmons, A., Soci, C., Abdalla, S., Abellan, X., Balsamo, G., Bechtold, P., Biavati, G., Bidlot, J., Bonavita, M., De Chiara, G., Dahlgren, P., Dee, D., Diamantakis, M., Dragani, R., Flemming, J., Forbes, R., Fuentes, M., Geer, A., Haimberger, L., Healy, S., Hogan, R.J., Hólm, E., Janisková, M., Keeley, S., Laloyaux, P., Lopez, P., Lupu, C., Radnoti, G., de Rosnay, P., Rozum, I., Vamborg, F., Villaume, S., Thépaut, J.N., 2020. The era5 global reanalysis. Quarterly Journal of the Royal Meteorological Society 146, 1999–2049. doi:10.1002/qj.3803.

Holton, J.R., 2004. An Introduction to Dynamic Meteorology. Elsevier Academic Press.

Ingrosso, R., Lionello, P., Miglietta, M.M., Salvadori, G., 2020. A statistical investigation of mesoscale precursors of significant tornadoes: The italian case study. Atmosphere 11, 301. doi:10-1002/joc.5526.

Kalnay, E., Kanamitsu, M., Kistler, R., Collins, W., Deaven, D., Gandin, L., Iredell, M., Saha, S., White, G., Woollen, J., Zhu, Y., Chelliah, M., Ebisuzaki, W., Higgins, W., Janowiak, J., Mo, K.C., Ropelewski, C., Wang, J., Leetmaa, A., Reynolds, R., Jenne, R., Joseph, D., 1996. The NCEP/NCAR 40-Year Reanalysis Project. Bulletin of the American Meteorological Society 77, 437–472. doi:10.1175/1520-0477(1996)077<0437:TNYRP>.0.CO;2.

Kaltenböck, R., Diendorfer, G., Dotzek, N., 2009. Evaluation of thunderstorm indices from ecmwf analyses, lightning data and severe storm reports. Atmospheric Research 93, 381 – 396. doi:https://doi.org/10.1016/j.atmosres.2008.11.005. 4th European Conference on Severe Storms.

Keul, A.G., Sioutas, M.V., Szilagyi, W., 2009. Prognosis of central-eastern mediterranean waterspouts. Atmospheric Research 93, 426 – 436. doi:https://doi.org/10.1016/j.atmosres.2008.10.028. 4th European Conference on Severe Storms.

Kirtman, B., Power, S., Adedoyin, J., Boer, G., Bojariu, R., Camilloni, I., Doblas-Reyes, F., Fiore, A., Kimoto, M., Meehl, G., Prather, M., Sarr, A., Schar, C., Sutton, R., van Oldenborgh, G., Vecchi, G., Wang, H., 2013. Near-term Climate Change: Projections and Predictability. Cambridge University Press. chapter 11. pp. 953—1028. doi:10.1017/CBO9781107415324.023.

Lawrence, M.G., 2005. The relationship between relative humidity and the dew-point temperature in moist air: A simple conversion and applications. Bulletin of the American Meteorological Society 86, 225–234. doi:10.1175/BAMS-86-2-225.

Markowski, P.M., Richardson, Y., 2010. Mesoscale Meteorology in Midlatitude. Wiley-Blackwell.

Markowski, P.M., Richardson, Y.P., 2014. The influence of environmental low-level shear and cold pools on tornadogenesis: Insights from idealized simulations. Journal of the Atmospheric Sciences 71, 243–275. URL: https://doi.org/10.1175/JAS-D-13-0159.1, doi:10.1175/JAS-D-13-0159.1.

Markowski, P.M., Straka, J.M., Rasmussen, E.N., 2002. Direct Surface Thermodynamic Observations within the Rear-Flank Downdrafts of Nontornadic and Tornadic Supercells. Monthly Weather Review 130, 1692–1721. doi:10.1175/1520-0493(2002)130<1692:DSTOWT>2.0.CO;2.

Marín, J.C., Barrett, B.S., Pozo, D., 2020. The tornadoes of 30–31 may 2019 in south-central chile: Sensitivity to topography and sst. Atmospheric Research , 105301doi:https://doi.org/10.1016/j.atmosres.2020.105301.

Matsangouras, I.T., Nastos, P.T., Bluestein, H.B., Sioutas, M.V., 2014. A climatology of tornadic activity over greece based on historical records. International Journal of Climatology 34, 2538–2555. doi:10.1002/joc.3857.

Meaden, J., 1976. Tornadoes in britain: Their intensities and distribution in space and time. The Journal of Meteorology 1, 242–251.

Miglietta, M., Mazon, J., Rotunno, R., 2017a. Numerical simulations of a tornadic supercell over the mediterranean. Weather and Forecasting 32, 1209–1226. doi:10.1175/WAF-D-16-0223.1.

Miglietta, M., Mazon, J., V., M., Pasini, A., 2017b. Effect of a positive sea surface temperature anomaly on a mediterranean tornadic supercell. Scientific Reports 7. doi:10.1038/595s41598-017-13170-0.

Miglietta, M.M., Matsangouras, I.T., 2018. An updated climatology of tornadoes and waterspout in italy. International Journal of Climatology , 1–17doi:10-1002/joc.5526.

Miglietta, M.M., Rotunno, R., 2016. An ef3 multivortex tornado over the ionian region: is it time for a dedicated warning system over italy. Bull. Amer. Meteor. Soc. 97, 337–344. doi:10.1175/BAMS-D-14-00227.1.

Molina, M.J., Allen, J.T., Prein, A.F., 2020. Moisture Attribution and Sensitivity Analysis of a Winter Tornado Outbreak. Weather and Forecasting 35, 1263–1288. doi:10.1175/WAF-D-19-0240.1.

Moncrieff, M.W., Miller, M.J., 1976. The dynamics and simulation of tropical cumulonimbus and squall lines. Quarterly Journal of the Royal Meteorological Society 102, 373–394. doi:10.1002/qj.49710243208.

Palmieri, S., Pulcini, A., 1978. Trombe d'aria sull'italia. Riv. Meteorol. Aeronaut. 4, 263–277.

Potter, S., 2007. Fine-tuning fujita: After 35 years, a new scale for rating tornadoes takes effect. Weatherwise 60, 64–

71. URL: https://doi.org/10.3200/WEWI.60.2.64-71, doi:10.3200/WEWI.60.2.64-71.

Púčik, T., Groenemeijer, P., Rýva, D., Kolář, M., 2015. Proximity soundings of severe and nonsevere thunderstorms in central europe. Monthly Weather Review 143, 4805–4821. doi:10.1175/MWR-D-15-0104.1.

Rasmussen, E.N., Blanchard, D.O., 1998. A baseline climatology of sounding-derived supercell and tornado forecast parameters. Weather and Forecasting 13, 1148–1164. doi:10.1175/1520-0434(1998)013<1148:ABCOSD>2.0.CO;2.

Renko, T., Kozarić, T., Tudor, M., 2013. An assessment of waterspout occurrence in the eastern adriatic basin in 2010: Synoptic and mesoscale environment and forecasting method. Atmospheric Research 123, 71 – 81. URL: http://www.sciencedirect.com/science/article/pii/S0169809512001937, doi:https://doi.org/10.1016/j.atmosres.2012.06.018. 6th European Conference on Severe Storms 2011. Palma de Mallorca, Spain.

Rodriguez, O., Bech, J., 2017. Sounding-derived parameters associated with tornadic storms in catalonia. International Journal of Climatology 38, 2400–2414. doi:10.1002/joc.5343.

Rodríguez, O., Bech, J., 2020. Tornadic environments in the iberian peninsula and the balearic islands based on era5 reanalysis. International Journal of Climatology n/a. doi:10.1002/joc.6825.

Romero, R., Gayà, M., Doswell, C.A., 2007. European climatology of severe convective storm environmental parameters: A test for significant tornado events. Atmospheric Research 83, 389 – 404.

doi:https://doi.org/10.1016/j.atmosres.2005.06.011. european Conference on Severe Storms 2004.

Romps, D.M., 2017. Exact expression for the lifting condensation level. Journal of the Atmospheric Sciences 74, 3551–3566.

Sioutas, M.V., Keul, A.G., 2007. Waterspouts of the adriatic, ionian and aegean sea and their meteorological environment. Atmospheric Research 83, 542 – 557. doi:https://doi.org/10.1016/j.atmosres.2005.08.009. european Conference on Severe Storms 2004.

Skliris, N., Sofianos, S.S., Gkanasos, A., Axaopoulos, P., Mantziafou, A., Vervatis, V., 2011. Long-term sea surface temperature variability in the aegean sea. Advances in Oceanography and Limnology 2, 125–139.

Taszarek, M., Allen, J.T., Púčik, T., Hoogewind, K.A., Brooks, H.E., 2020. Severe convective storms across Europe and the United States. Part 2: ERA5 environments associated with lightning, large hail, severe wind and tornadoes. Journal of Climate , 1–53URL: https://doi.org/10.1175/JCLI-D-20-0346.1, doi:10.1175/JCLI-D-20-0346.1.

Taszarek, M., Brooks, H.E., Czernecki, B., 2017. Sounding-Derived Parameters Associated with Convective Hazards in Europe. Monthly Weather Review 145, 1511–1528. doi:10.1175/MWR-D-16-0384.1.

Taszarek, M., Brooks, H.E., Czernecki, B., Szuster, P., Fortuniak, K., 2018. Climatological aspects of convective parameters over europe: A comparison of era-interim and sounding data. Journal of Climate 31, 4281–4308.

URL: https://doi.org/10.1175/JCLI-D-17-0596.1, doi:10.1175/JCLI-D-17-0596.1.

Taszarek, M., Kolendowicz, L., 2013. Sounding-derived parameters associated with tornado occurrence in poland and universal tornadic index. Atmospheric Research 134, 186 – 197. doi:https://doi.org/10.1016/j.atmosres.2013.07.016.

Thompson, R.L., Edwards, R., Hart, J.A., 2003. Close proximity soundings within supercell environments obtained from the rapid update cycle. Weather and forecasting 18, 1243–1261. doi:10.1175/1520-0434(2003)018¡1243:CPSWSE¿2.0.CO;2.

Uppala, S.M., KÅllberg, P.W., Simmons, A.J., Andrae, U., Bechtold, V.D.C., Fiorino, M., Gibson, J.K., Haseler, J., Hernandez, A., Kelly, G.A., Li, X., Onogi, K., Saarinen, S., Sokka, N., Allan, R.P., Andersson, E., Arpe, K., Balmaseda, M.A., Beljaars, A.C.M., Berg, L.V.D., Bidlot, J., Bormann, N., Caires, S., Chevallier, F., Dethof, A., Dragosavac, M., Fisher, M., Fuentes, M., Hagemann, S., Hólm, E., Hoskins, B.J., Isaksen, L., Janssen, P.A.E.M., Jenne, R., Mcnally, A.P., Mahfouf, J.F., Morcrette, J.J., Rayner, N.A., Saunders, R.W., Simon, P., Sterl, A., Trenberth, K.E., Untch, A., Vasiljevic, D., Viterbo, P., Woollen, J., 2005. The era-40 re-analysis. Quarterly Journal of the Royal Meteorological Society 131, 2961–3012. doi:10.1256/qj.04.176.

Zanini, M.A., Hofer1, L., Faleschini1, F., Pellegrino, C., 2017. Building damage assessment after the riviera del brenta tornado, northeast italy. Natural Hazards 86, 1247–1273. doi:10.1007/s11069-017-2741-6.